EUROfusion

EUROFUSION WPJET1–PR(15)01

M. Lennholm et al.

Real-Time Control of ELM and Sawtooth Frequencies: Similarities and Differences

Preprint of Paper to be submitted for publication in
Nuclear Fusion

This work has been carried out within the framework of the EUROfusion Consortium and has received funding from the Euratom research and training programme 2014-2018 under grant agreement No 633053. The views and opinions expressed herein do not necessarily reflect those of the European Commission.

Real-Time Control of ELM and Sawtooth Frequencies: Similarities and Differences.

M.Lennholm[1,2], D.Frigione[3], J.Graves[4], P.S.Beaumont[5], T.Blackman[5], I.S.Carvalho[6], I.Chapman[5], R.Dumont[7], R.Felton[5], L.Garzotti[5], M.Goniche[7], A.Goodyear[5], D.Grist[5], S.Jachmich[8,2], T.Johnson[9], P.Lang[10], E.Lerche[8,5], E.de la Luna[11], I.Monakhov[5], R.Mooney[5], J.Morris[5], M.F.F.Nave[6], M.Reich[10], F.Rimini[5], G.Sips[1,2], H.Sheikh[5], C.Sozzi[12], M.Tsalas[13,5] and JET contributors*

EUROfusion Consortium, JET, Culham Science Centre, Abingdon, OX14 3DB, UK

[1]European Commission, B-1049 Brussels, Belgium;
[2]EFDA Close Support Unit, Culham Science Centre, Abingdon, OX14 3DB, UK;
[3]ENEA, C.R. Frascati, Roma, Italy;
[4]EPFL, CRPP, CH-1015 Lausanne, Switzerland;
[5]CCFE, Culham Science Centre, Abingdon, OX14 3DB, UK;
[6]Instituto de Plasmas e Fusão Nuclear, Instituto Superior Técnico, Universidade de Lisboa, P-1049-001 Lisboa, Portugal;
[7]CEA, IRFM, F-13108 Saint-Paul-lez-Durance, France;
[8]Laboratory for Plasma Physics, Koninklijke Militaire School - Ecole Royale Militaire Renaissancelaan 30 Avenue de la Renaissance B-1000 Brussels Belgium;
[9]VR, Fusion Plasma Physics, EES, KTH, SE-10044 Stockholm, Sweden;
[10]Max-Planck-Institut für Plasmaphysik, D-85748 Garching, Germany;
[11]Laboratorio Nacional de Fusion, CIEMAT, Madrid, Spain;
[12]IFP-CNR, via R. Cozzi 53, 20125 Milano, Italy;
[13]FOM Institute DIFFER P.O. Box 1207 NL-3430 BE Nieuwegein, The Netherlands

*See the Appendix of F. Romanelli et al., Proceedings of the 25th IAEA Fusion Energy Conference 2014, Saint Petersburg, Russia

E-mail contact of main author: morten.lennholm@jet.uk

Abstract. ELMs and Sawteeth, located in different parts of the plasma, are similar from a control engineering point of view. Both manifest themselves through quiescent periods interrupted by periodic collapses. For both, large collapses, following long quiescent periods, have detrimental effects while short periods are associated with decreased confinement. Following the installation of the all metal 'ITER like wall' on JET, sawteeth and ELMs also play an important role by expelling tungsten from the core and edge of the plasma respectively. Control of tungsten has therefore been added to divertor heat load reduction, NTM avoidance and helium ash removal as reasons for requiring ELM and sawtooth control. It is therefore of interest to implement control systems to maintain the sawtooth and ELM frequencies in the desired ranges. On JET, ELM frequency control uses radial field 'kicks' and pellet and gas injection as actuators, while sawtooth control uses Ion Cyclotron Resonance Heating (ICRH). JET experiments have, for the first time, established feedback control of the ELM frequency, via real time variation of the injected gas flow [1]. Using this controller in conjunction with pellet injection allows the ELM frequency to be kept as required despite variations in pellet ELM triggering efficiency. JET Sawtooth control experiments have, for the first time, demonstrated that low field side ICRH, as foreseen for ITER, can shorten sawteeth lengthened by central fast ions [2]. The development of ELM and sawtooth control could be key to achieve stable high performance JET discharges with minimal tungsten content. Integrating such schemes into an overall control strategy will be required in future tokamaks and gaining experience on current tokamaks is essential.

1. Introduction

Maintaining the frequency of both ELMs [3-7] and sawteeth [8-16] in a desired range is required for stable high performance tokamak operation. Long period sawteeth are likely to trigger neoclassical tearing modes (NTMs), while large infrequent ELMs are likely to cause unacceptable heat loads. At the same time frequent sawteeth and ELMs are instrumental in expelling heavy impurities from the plasma core and edge respectively. One of the main challenges facing JET operation, following the installation of the all metal 'ITER like wall' [45-48], is to avoid accumulation of tungsten in the plasma centre [49-52] and sawtooth and here ELMs play an important role. While ELMs, if they occur sufficiently frequently, can expel tungsten from the plasma edge before it penetrates deeper into the plasma [51], sawteeth will expel tungsten from the plasma centre towards the outer regions [2][53]. Moderately high ELM and sawtooth frequencies are therefore required to maintain an acceptable tungsten concentration in the plasma. On the other hand increasing the sawtooth and ELM frequencies in general leads to a degradation of the confinement. ELM and Sawtooth control therefore aims at achieving frequencies that are high enough to avoid tungsten accumulation, NTMs and excessive heat loads, without paying too high a price in terms of confinement.

2. Control Strategy

The bursting nature of sawteeth and ELMs means that two distinct control strategies can be considered. In pacing/locking control, exemplified by pellet ELM triggering [21-24] and Radial Field 'kicks' [25-29], the plasma is perturbed periodically at the desired frequency. Continuous control schemes, exemplified by Electron or Ion Cyclotron heating control of sawteeth [30-44], modify the underlying plasma parameters which determine the collapse frequency. In this case a permanent perturbation is applied and certain properties of this perturbation are adjusted to achieve the desired ELM or Sawtooth frequency. These two approaches are described in more details below.

2.1. Pacing and Locking

In this approach, as already mentioned, perturbations are applied periodically. If these perturbations are sufficiently large, each perturbation will trigger either an ELM or a sawtooth crash. This kind of control is normally described as ELM or sawtooth pacing. To use more accurate language, applying perturbations with pre-programmed intervals between the perturbations is more correctly described as period locking. Pacing, on the other hand, refers to the situation where the perturbation is initiated a certain pre-programmed time after the previous ELM or sawtooth crash. In the case of pacing and for certain types of perturbations, the perturbation can be maintained or increased until an ELM or a sawtooth crash is triggered. The advantage of the locking approach is that, in principle, no real time measurement of the ELM or Sawtooth period is required. On the other hand, having no real time measurement of the response to the perturbation means that there is no way of knowing whether the ELM/sawtooth frequency actually lock to the perturbation frequency. It is clearly desirable to know whether the locking works reliably, so that the applied perturbation can be adjusted on a slower time scale to assure reliable control. Though locking looks an attractive option due to the fact that no real time control is required, pacing is likely to be much more robust, especially if the amplitude of each perturbation can be increased until an ELM or a sawtooth crash is triggered. The difficulty in the case of pacing is that the detection of ELMs and

sawtooth crashes has to be very reliable and the ELM or sawtooth crash must not be confused with the effect on the measurement of the perturbation itself. Figure 1 shows a schematic representation of pacing and locking controllers.

2.2. Continuous Controllers

In this approach the burst frequency is controlled by changing the underlying physics parameters responsible for the ELM or sawtooth period. To achieve the desired change in the underlying parameters the control actuators are adjusted in a continuous way. In most cases the actuators used will be applied continuously, though pulsed application can also be used in this control mode and it will still be considered continuous control as long as the pulses are not synchronised with the ELMs or the sawteeth. If the plasma parameters are very stable throughout, it is possible that pre-programming the actuators can do the job but such stability is not very likely, especially since the ELM and sawtooth periods are strongly affected by a number of unforeseeable perturbations. It is therefore likely that achieving the desired results requires that certain actuator parameters are changed through a closed loop control, responding to variations in the plasma parameters. To implement a successful closed loop controller it is essential to have a reliable real time measurement of the ELM or sawtooth period and other relevant underlying parameters. Such real time detection will be treated in more detail in section 4. The role of these controllers is to reject disturbances efficiently. As opposed to most control problems, the required precision with which the desired frequency is achieved is not very stringent. The most important role of the controller is to assure that the ELM or Sawtooth period does not exceed a certain maximum period as even one long interval between ELMs or sawtooth crashes is likely to have detrimental effects. Figure 2 shows a simple continuous control block diagram. More details of various continuous controllers will be given in section 5.

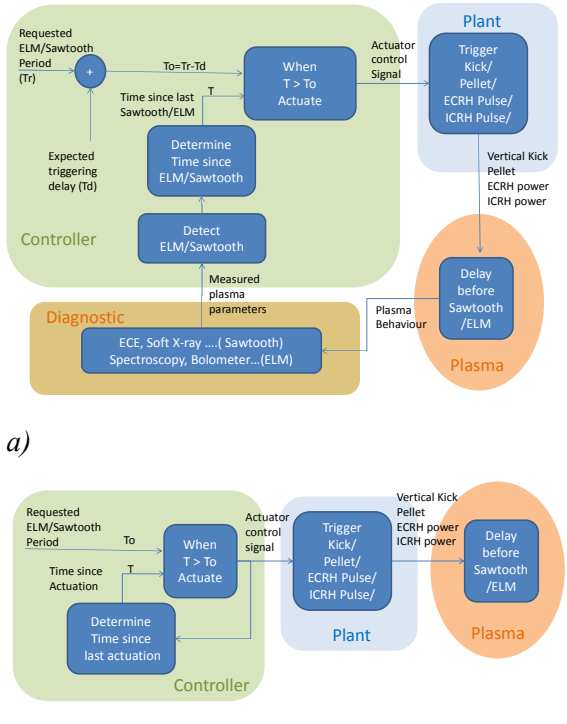

Figure 1. Pacing and Locking controllers.

Of the various control options described above, both sawtooth pacing and sawtooth locking have been demonstrated on TCV [54-56] and the difference in the parameter range over which these two types of control can be efficient is assessed. ELM pacing and locking

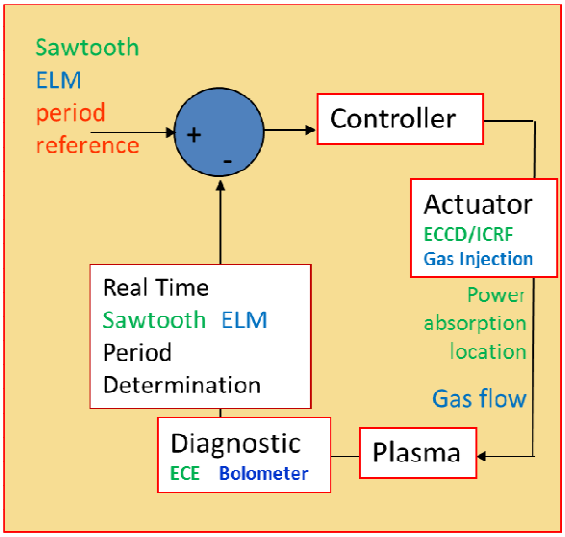

Figure 2. Continuous Controllers.

has been achieved on JET and on various other machines and results on ELM pacing on JET will be given in section 6 [21-29]. Open loop 'continuous' sawtooth frequency control on JET, TCV and ASDEX-Upgrade is described in [30-34], [35] and [36] respectively, while closed loop sawtooth frequency control has been demonstrated on JET [44], Tore Supra [39-40] and TCV [41-43]. Meanwhile the recent closed loop ELM frequency control experiments described in more detail in section 6 constitute the first demonstration of such a control scheme [1].

3. Actuators

The choice of actuators depends on the control strategy and is obviously different for sawtooth and ELM control. ELM pacing or locking has been demonstrated using either the injection of small pellets or the application of so-called 'radial field kicks' [21-29]. Continuous ELM frequency control can use a variety of actuators, notably gas injection [57-59], impurity injection and the application of toroidally asymmetric fields [60-64]. For sawtooth control the main actuators are the injection of either electron or ion cyclotron waves, which can be used either pulsed to achieve sawtooth pacing or continuously for open or closed loop control [2] [30-44][54-56]. These actuators and their potential for ELM and sawtooth control are assessed in the following.

3.1. ELM pacing and triggering

The application of so-called radial field 'kicks' has been seen to be able to trigger ELMs. A radial field 'kick' is a short duration, fast, variation in the radial field. With the right duration and rate of change of the radial field, ELMs can be triggered with high reliability. The advantage of using radial field kicks to trigger ELMs is that the control is achieved with minimum impact on the general plasma performance. On the other hand the plasma will accelerate vertically during a 'kick' and as the plasma is vertically unstable the system responsible for maintaining vertical stability may not be able to stop this vertical movement following a 'kick'. In this case a so-called vertical displacement event (VDE) will take place and the plasma will disrupt as it rams into the vacuum vessel. Such VDE's are associated with large forces which can potentially damage the vacuum vessel and other tokamak components [65]. The added risk of causing VDE's associated with radial field kicks means that such kicks are unlikely to be useful for ELM control in high current JET pulses and even less in

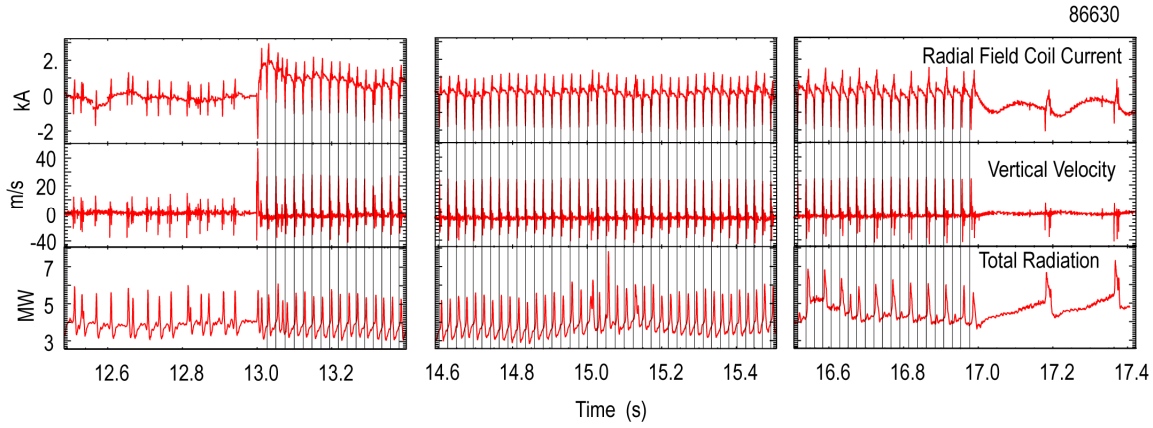

Figure 3. Vertical 'kick' ELM triggering. Vertical black lines indicate the times of the 'kicks'. Most 'kicks' trigger ELMS in the first two time windows. In the third time window only half of the 'kick' trigger ELMs.

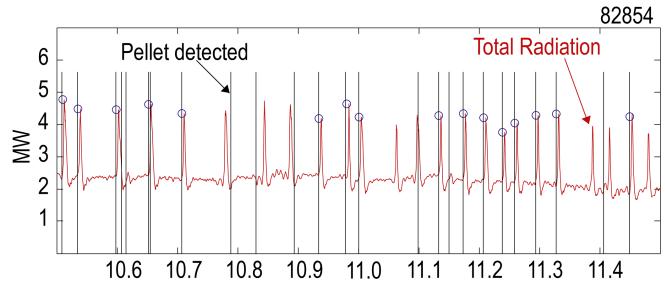

Figure 4. Pellet ELM triggering. Circles indicate triggered ELMs. Pellets very close together are pellet fragments.

high performance ITER plasmas. Radial field kicks have been used in a number of JET experiments over recent years and both ELM pacing and ELM frequency locking has been demonstrated. An example of the ELM frequency being locked to the radial field kick frequency in a recent JET pulse is seen in figure 3. Three different time windows during this pulse are shown. The first window shows how the natural ELM frequency is increased as soon as the 'kicks' are started. A couple of extra ELMs are triggered before complete synchronization is achieved. The second time window shows good synchronization throughout. In the third time window, only half of the kicks succeed in triggering ELMs. When the 'kicks' are stopped it is seen that the natural ELM frequency has become far lower than it was when the 'kicks' started. This illustrates that the achievable ELM frequency is dependent on the natural frequency. It is possible that increasing the size of the 'kicks' could have assured that the higher ELM frequency had been maintained. A secondary control could possibly have been used to increase the kick size once it was detected that the ELM triggering became unreliable. This would, however, have increased the vertical velocity perturbation. This perturbation, seen in the second trace in figure 3 is, already about twice the perturbation associated with natural ELMs and a further increase is unlikely to be desirable.

The second method which has been seen to be promising for ELM frequency pacing/locking, is the injection of small pellets of frozen deuterium into the plasma. If these pellets are large and fast enough they induce ELMs with good reliability as demonstrated on a number of tokamaks [21-24]. Depending on the type and performance of the pellet injector, pellets arrive at the plasma more or less regularly and for the JET experiments the pellets are not arriving with very precise intervals into the plasma. The flight time of the pellets from the pellet injector to the plasma is also so long that, when pellet frequencies in the 10-50Hz range are used, several pellets will be on their way through the pellet flight lines at the same time. The significant time that it takes for pellets to reach the plasma means that there is no way of affecting the time a pellet reaches the plasma in response to the timing of the last ELM. For this reason ELM pacing, in the sense defined above, is not possible and, given the irregularity of the interval between pellets, even ELM frequency locking is not really the correct term. It is more correct to talk about repetitive ELM triggering. Figure 4 shows a JET pulse in which a number of ELMs are triggered by pellets. Not all ELMs during the pellet injection interval are triggered by pellets and not all pellets trigger ELMs. In addition the injection of pellets also changes the underlying plasma parameters – notably the edge pressure – and therefore injection of pellets also affect the natural ELM frequency in a similar way to gas injection as described in the subsequent paragraph.

3.2. Continuous Actuators for ELM Frequency Control

A number of different actuators can be used to change the underlying physics parameters which determine the ELM frequency. The two most obvious of these are additional heating power [66]– on JET principally neutral beam injection (NBI) power – and the amount of gas

injected into the tokamak vacuum vessel. When operating in the 'Type-I ELMy H-mode' operational space the ELM frequency increases with heating power. In the type-I regime the ELM frequency also usually increases with increased gas injection until the type of ELMs change to high frequency 'type-III ELMs'. The frequency of type III ELMs decrease, rather than increase, with injected NBI power, whereas the effect of increasing the gas injection is less clear though a sufficient increase in the gas injection eventually leads to the plasma returning to L-mode where there are no ELMs. The current paper only considers the control of Type-I ELMs and hence the control schemes developed should avoid pushing the plasma into the Type-III regime. Though varying the power is very efficient in changing the ELM frequency, the power is normally determined by other requirements and it is hence not an ideal control actuator for ELM frequency control. Gas injection is, on the other hand, more attractive to use as a control actuator. The development of such a controller is described in some detail in [1]. The essential elements of this work are described below and some examples of the use of the controller in specific experiments are given in section 6. Two characteristics of the way gas injection affects the ELM frequency are important for the development of a closed loop controller:

i) The gas flows from the gas injection modules (GIMs) to the vacuum vessel through fairly long pipes – leading to a significant delay (200-500ms for JET) from changing the GIM opening until the effect is seen on the plasma.
ii) The reaction of the ELM frequency to a change in gas injection can be non-linear.

Figure 5 shows an open loop step response experiment where the gas injection rate is changed abruptly from $0.5 \cdot 10^{23}$ electrons/s to $1.2 \cdot 10^{23}$ electrons/s. This figure illustrates the delay in the ELM frequency response. Figure 6 shows the ELM period (the inverse of the ELM frequency) as a function of the gas injection rate, showing the strong non-linearity. The points inthis figure are taken from 6 discharges similar to the one in figure 5. The scatter within individual discharges is due to the irregular nature of the ELMs, while the systematic differences between different discharges is related to other parameters, notably NBI power and plasma density. The figure includes two trend curves, with the blue curve shifted rigidly to the right by $1.0 \cdot 10^{22}$ electrons/s with respect to the magenta curve.
Various other actuators can be used to affect the ELM frequency. One of the most promising of these is the application of non-axis-symmetric magnetic fields. A number of experiments on JET using the JET Error Field coils [64] and on other machines such as D-IIID and ASDEX-Upgrade have demonstrated how the ELM frequency can be modified by such coils

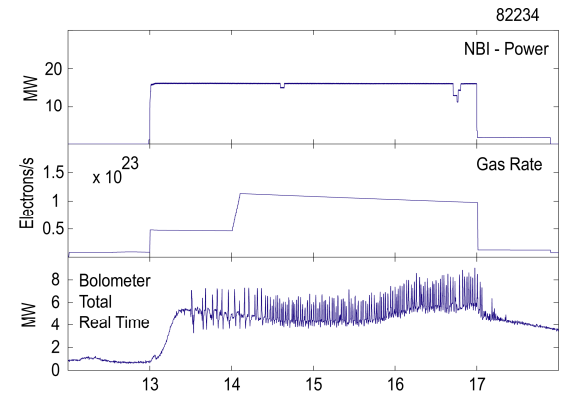

Figure 5. The response of the ELMs to a variation in gas injection rate.

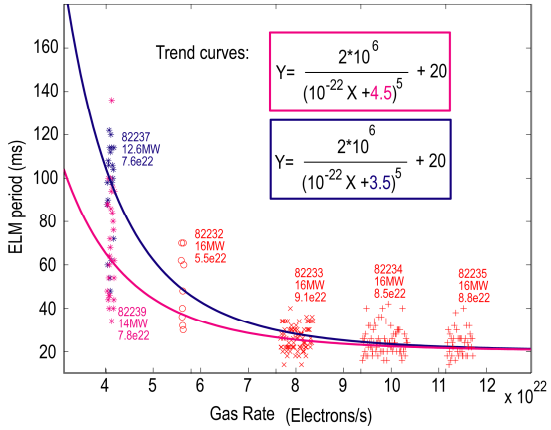

Figure 6. ELM period as a function of gas injection rate.

[60-63]. In some experiments the ELMs have even been completely eliminated using this method, while remaining in H-mode. To the knowledge of the authors no closed loop schemes have been developed for control of the ELM frequency through variation of the current in such ELM control coils, though implementing such control certainly seems feasible. A final actuator, which should be mentioned, is the injection of impurities as this also strongly affects the ELM frequency. Whether impurity injection would be a good actuator for ELM control is questionable as impurity injection is likely to be used to control other parameters, such as edge radiation, and it is therefore more likely that impurity injection will have to be treated as a disturbance by a closed loop ELM frequency controller.

3.3. Actuators for Sawtooth Frequency Control

Sawtooth frequency feedback control and pacing/locking would both use ECRH and/or ICRH. For pacing/locking the power would be 'on – off' modulated at the required frequency, while continuous feedback controllers would change the ICRH frequency and/or the ECRH injection angle in real time. It is likely that, even for sawtooth pacing, some real time control of the ECRH/ICRH absorption location and power would be required. ECRH has been used on TCV to demonstrate both sawtooth pacing and locking [54-56]. So far these pacing/locking experiments have not demonstrated the shortening of the sawtooth period below the natural period without the application of the modulated ECRH.

The development of continuous closed loop schemes for sawtooth period control using variation of the ECRH injection angle as the actuator has been extensively studied on Tore Supra and TCV [39-43]. In the Tore Supra experiments the main performance limitation was imposed by the speed with which the Tore Supra ECRH mirrors could be moved. This imposed a response time of about 1s. The Tore Supra antenna and associated controllers have recently been updated [66] to significantly improve this response time, which promises to allow much better sawtooth control performance when Tore Supra starts operating again after its upgrade through the WEST project [67].

The ability of precisely located ion cyclotron resonant heating (ICRH) to strongly affect the sawtooth period have been demonstrated in a number of JET experiments [30-34]. In most of these experiments the ICRH absorption was located on the High Field Side and in this case it was seen that:

i) The ICRH waves had to be injected with a preferred toroidal propagation direction ($N_{\|}$). This was achieved by operating the JET antennas with a specific phasing between the individual straps in the JET four strap antenna.
ii) The Ion Cyclotron resonance position had to be located with great precision with respect to the q=1 surface, where q is the safety factor.

Based on the high sensitivity of the sawtooth period to the precise location of the ion cyclotron resonance location, a closed loop sawtooth frequency controller, using the ICRH frequency as the actuator, was developed at JET [44]. By varying this ICRH frequency the location of the ion cyclotron resonance could be moved. Though demonstrating the feasibility of using the ICRH frequency as the actuator these experiments suffered from a number of limitations associated with the ability of varying the ICRH frequency. The speed of variation of the ICRH frequency and the range over which this frequency can be varied is limited by the

requirement that the RF generator has to be matched to the transmission line-antenna-plasma ensemble.

To maintain this match when the ICRH frequency and thereby the wavelength changes, the length of the transmission lines have to change such that their length measured in number of wavelengths remain constant. To achieve this, large elements referred to as 'trombones' are moved. The trombones can vary the transmission line length by +- 1.5m but the movement of these trombones is rather slow and the full stroke of movement takes approximately 10s. An automatic matching system which forms part of the ICRH plant detects any mismatch and moves the trombones to recover the matching.

The controller used in the experiments presented in [44] generated a frequency offset which was sent to the ICRH plant, where it was added to the nominal operation frequency. As the RF transmission line – antenna system is a highly resonant structure, the change in operation frequency leads to a mismatch, which in turn results in increased power reflected back to the RF generator. The internal matching system within the ICRH plant compensates for this mismatch by moving the trombones, varying the trombone speed as a function of the observed mismatch using a simple proportional controller. An added complication, which is not mentioned in [44], is that the trombone speed can only be varied in five steps (- fast, - slow, 0, + slow, + fast). This means that, in order to make the trombone move at all a significant mismatch has to exist. This mismatch has to be even larger to assure that the trombone moves at its maximum speed. At the same time the mismatch must not be too large as this causes the RF generator to be switched off. This problem, described in more detail in [44] means that it is necessary to know the position of the matching trombones in real time. As no real time measurement of this position is available, a real time simulation was used to get this information. The control scheme used in [44] resulted in the generator operating continuously with significant reflected power. This in turn limited the maximum power which could be coupled to the plasma.

Based on a detailed analysis of the ICRH matching system, described in more detail in section 3.3.1, an alternative ICRH frequency control algorithm allowing improved RF plant matching has been developed as described in section 3.3.2. As the RF matching is the most challenging aspect of the implementation of real time RF control, the background for this matching is analysed in some detail in the following.

3.3.1. ICRH automatic matching

To understand how good matching can be maintained while changing the ICRH frequency it is useful to analyse the operation of the automatic matching in more detail. Figure 7a shows the principle of how this automatic matching works in the normal mode of operation. The RF frequency is fixed or controlled externally and the RF generator emits power into the coaxial transmission lines which guide the RF wave to the antenna, from where the RF power is radiated towards the plasma. In order to avoid any power being reflected towards the generator, the resistance seen at the output of the generator has to be the same as the characteristic impedance Z_C of this transmission-line, which in the JET case is $Z_C = 30\Omega$. The antenna, on the other hand presents a resistance, known as the coupling resistance R_C of the order of a few Ohm, to the transmission line. As a consequence significant power would be reflected towards the generator if the antenna was connected to the end of the transmission line without further measures. The role of the stub and trombone seen in figure 7 is to

transform the impedance Z_{load} seen by the generator to achieve $Z_{load} = Z_C$. The stub is a piece of coaxial transmission line which is terminated by a short circuit. The length of this stub can be varied, thereby varying the admittance Y_{stub} seen from the T-junction towards the stub. Here $Y_{stub} = \frac{1}{Z_{stub}}$ where Z_{stub} is the complex impedance of the stub. The trombone is a piece of transmission line with variable length. Varying the trombone length changes the admittance $Y_{tr} = \frac{1}{Z_{tr}}$ seen from the T-junction towards the antenna. The admittance which the T-Junction presents to the transmission line between the generator and the T-junction is $Y_{T-junction} = Y_{stub} + Y_{tr}$. By setting the stub and trombone lengths appropriately one can achieve $Y_{T-junction} = \frac{1}{Z_C}$. Transforming the load seen at the T-junction back to the generator does not change this load, as long as the load is equal to the characteristic transmission line impedance, and thus we achieve $Z_{load} = Z_C$ as desired.

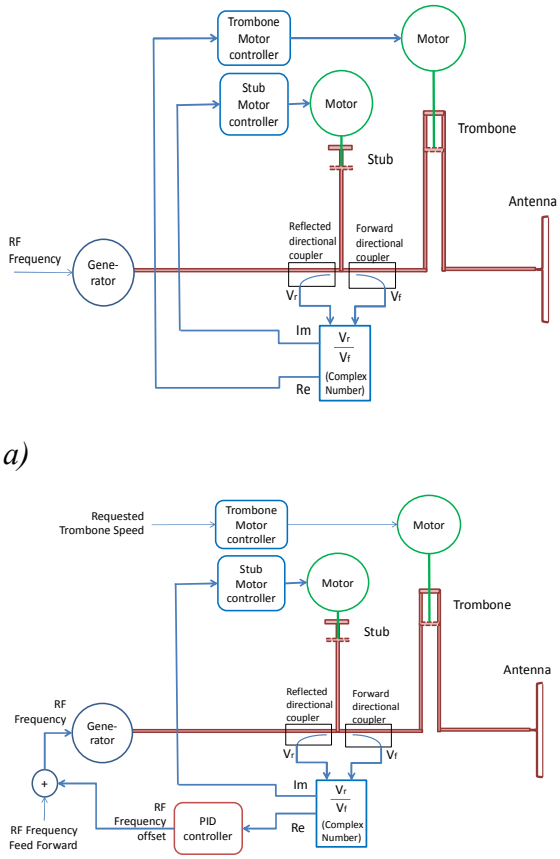

Figure 7:

a) ICRH automatic matching. Transmission lines, Antenna and matching elements (Stub and Trombone) are shown in red.

b) Alternative ICRH automatic matching. The RF frequency rather than the trombone is used as the actuator to control $\mathrm{Re}\left(\frac{V_r}{V_f}\right)$.

Another way to view this is in terms of transmitted and reflected waves. Three waves travel towards the T-Junction:

i) The wave coming from the Generator: W_{GF}

ii) The wave returning towards the T-junction after reflection at the short at the end of the stub W_{SR}

iii) The wave returning towards the T-junction after reflection at the antenna W_{AR}

Here W_{GF}, W_{SR} and W_{AR} are complex numbers representing the amplitude and phase of the respective waves. These waves will be partly transmitted and partly reflected at the T-junction. The wave W_{GR} travelling from the T-junction back towards the generator is

$$W_{GR} = R_G W_{GF} + T_{SG} W_{SR} + T_{AG} W_{AR}$$

Here R_G is the reflection coefficient of the T-junction as seen from the generator, while T_{SG} and T_{AG} are the transmission coefficients through the T-junction for waves coming back from the stub and antenna respectively.

The aim of setting the length of the stub and trombone is now to assure that the phases and amplitudes of the three waves $R_G W_{GF}$, $T_{SG} W_{SR}$ and $T_{AG} W_{AR}$ are such that they cancel each other to achieve $W_{GR} = 0$. As the amplitude of the waves reflected from stub and antenna are large, the cancelation depends strongly on the relative phases of these waves. When a perfect match is obtained, the transmission line circuit between the short circuit at the end of the stub and the antenna behaves as a high Q resonant circuit, with power being 'pumped in' from the generator and then lost from the circuit mainly through radiation from the antenna. During operation at constant frequency the coupling resistance R_C varies and the automatic matching responds by changing stub and trombone lengths to maintain $W_{GR} = 0$.

The matching control loop used at JET is seen in figure 7a. Two directional couplers are used to measure the amplitude and phase of the waves traveling from the T-junction towards the antenna and back towards the generator respectively. The measurements are translated into the complex numbers V_f and V_r, containing the amplitude and phase information, before producing the complex ratio $\frac{V_r}{V_f}$. This ratio can be split into its real and imaginary parts and the aim of the controller is to bring both the imaginary and real part to zero. Though both stub and trombone lengths affect both real and imaginary parts of $\frac{V_r}{V_f}$ the stub mainly affects the imaginary part while the trombone length mainly affects the real part. This is the basis for the matching controller. Once $\frac{V_r}{V_f}$ is generated, its imaginary part is used as the error signal for the stub control loop, while the real part is used as the error signal for the trombone position controller. As both imaginary and real values can take both negative and positive values this controller is effective in bringing both the imaginary and real part to zero and as a consequence V_r itself becomes zero, indicating that no power is reflected towards the generator.

The sawtooth controller described in [44] used the generator frequency as the control actuator. As described earlier, a change in frequency affects the phase of the waves returning towards the T-junction from the stub and antenna. As the length of the transmission line between the T-junction and the antenna is much longer than the length of the stub the phase change will be dominated by the wave reflected from the antenna. To fully compensate the phase change caused by a change in frequency, movement of both the trombone and the stub is required. For the small frequency changes available for the real time controller, the required stub movement is virtually negligible and the compensation is therefore done by moving the trombone only.

As already mentioned the stepwise control of the trombone motors means that, if the fastest possible frequency variation and therefore the fastest trombone movement is required, the trombone error signal $\mathrm{Re}\left(\frac{V_r}{V_f}\right)$ has to be rather large. This means that significant power is reflected towards the generator. Only one of the JET RF generators can work with such high reflection. The tolerance is due to the way this specific generator is used to feed two separate antennae via a 3dB coupler. The 3dB coupler is tuned such that the power reflected from the two antennae is directed into a dummy load rather than back towards the generator itself. This was exploited in the experiments presented in [44] where only the specific generator in question was used, limiting the available generator power to less than half of the power which would be available if operating with high reflection would not be required.

3.3.2. Alternative Real Time ICRH Frequency Control Scheme

To allow RF frequency variation on all the JET RF generators, an alternative scheme for controlling the generator frequency has been developed. The basic idea of this control scheme is to allow the sawtooth controller to take control of the trombone movement, letting the internal matching system respond by changing the RF frequency, to control $\mathrm{Re}\left(\frac{V_r}{V_f}\right)$ to zero. Figure 7b illustrates this matching scheme. The controller in this case is a continuous PID controller which means that it reacts even to small values of $\mathrm{Re}\left(\frac{V_r}{V_f}\right)$. In addition the RF frequency, can respond much faster than the trombone. Exploiting this internal matching, a new way of varying the RF frequency from an external signal was devised. To achieve this, new cabling was put into the ICRH plant to allow the trombone controllers to receive an external signal generated by the JET real time central controller (RTCC) [68].

Initial tests of this new indirect frequency control are shown in figure 8. In these tests, the trombone was requested to move at its maximum speed for about 7 seconds. The figure shows that the trombone starts moving in response to this request, with a delay of approximately 0.7s. This delay clearly reduces the performance in closed loop operation and the cause of the delay is being investigated. Once the trombone is moving, the frequency control loop is seen to respond immediately, maintaining the error signal near zero. The bottom trace shows how the voltage reflection coefficient seen by the generator is kept well below 0.1. This reflection coefficient is defined as the ratio of the absolute values of forward and reflected voltages at the output of the generator. The reflection coefficient is non-zero, as a consequence of the stubs not being used for matching in the test and hence $\mathrm{Im}\left(\frac{V_r}{V_f}\right)$ is not controlled to zero. The loss of power from the generator between 7.5s and 8.5s, is due to the added complication of

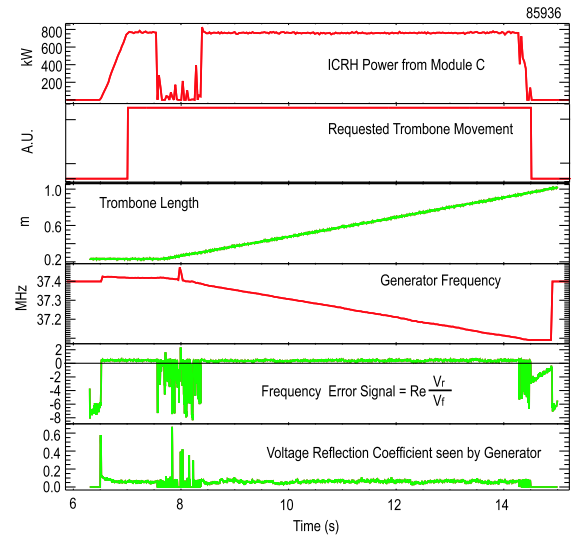

Figure 8: Feed forward test of alternative frequency control scheme. The trombone is requested to move at constant (maximum) speed and the frequency responds, maintaining the match.

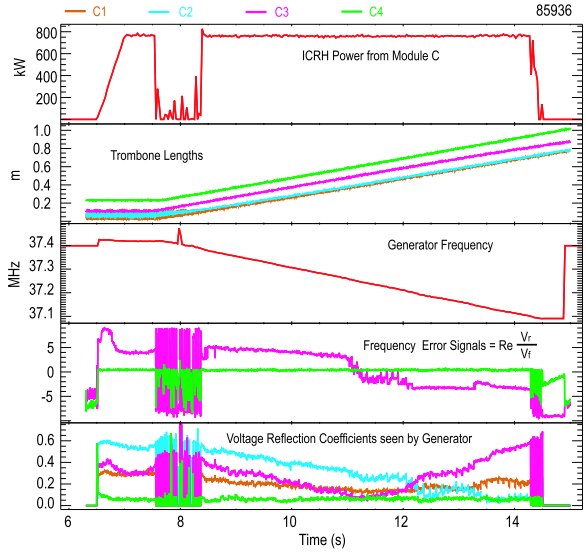

Figure 9: Trombone positions and reflection coefficients for all 4 transmission lines from generator C for the discharge in figure 8. For clarity only two 'frequency error signals' are shown.

one generator powering four separate transmission lines, feeding four antenna straps, each of which needs to be reasonably well matched. As the output frequency from a generator is the same for all four outputs, the frequency can only be used to match one of these transmission lines. While each transmission line is equipped with a trombone (and a stub) only one trombone velocity request signal is available for the real time controller. This means that all four trombones are requested to move at the same velocity.

Figure 9 illustrates the consequences of this in the discharge from figure 8. As can be seen in the second panel, the four trombones move at almost identical velocities. The fourth panel shows the evolutions of $\mathrm{Re}\left(\frac{V_r}{V_f}\right)$ for the third and fourth output (for clarity the traces for the first and second output have been omitted in this panel). The fourth output (green) is the one used by the matching controller and as already seen in figure 9 this trace is controlled to remain near zero. The third output (magenta), on the other hand, is not controlled in a closed loop, and this therefore is not maintained at zero. This signal is positive in the beginning of the discharge – indicating that the trombone is too long (or the frequency is too high). Towards the end of the discharge $\mathrm{Re}\left(\frac{V_r}{V_f}\right)$ for the third output rapidly passes through zero and becomes negative indicating that this trombone, at the end of the test, is too short (or the frequency too low).

This illustrates that, rather than all trombones moving at the same speed, matching requires them to move at different speeds. This is due to the fact that the different transmission lines do not have the same length and hence a change in frequency, leads to different changes in reflected phase for the different transmission lines. In the bottom panel in figure 9 it is seen how the four reflection coefficients, seen from the generator, varies as the frequency changes and the trombones move. Only the fourth output remains well matched throughout. The reflection coefficient for the second output (turquoise) reaches 0.6, which is the maximum allowed, between 7.5s and 8.5s causing the observed power trip. At about 14.3s the third output (magenta) reaches this maximum, again causing the power to trip.

To remedy this problem another feature of the ICRH plant is exploited. In fact each transmission line is equipped with two trombones mounted in series. One of these is long but can only move rather slowly. The other trombone is short but significantly faster. The fast trombones are too short to allow sufficient frequency variation as required for sawtooth control. They are, however, sufficiently long to be able to recover the mismatch caused by forcing all the slow trombones to move together. In this modified frequency control scheme, the external trombone request moves all the slow trombones in unison. The internal matching system varies the generator frequency to match one of the four outputs. For the other three outputs the internal matching system uses the fast trombones to control $\mathrm{Re}\left(\frac{V_r}{V_f}\right)$ to zero. As the main trombones for these three outputs are feed-forward controlled together to move at the same rate as the trombone for which the movement is compensated through frequency variation, the length variations required from the additional short trombones are modest.

Figure 10 shows the principle of this mode of operation, while figure 11 shows the resulting frequency control. For simplicity, only signals associated with two out of four generator

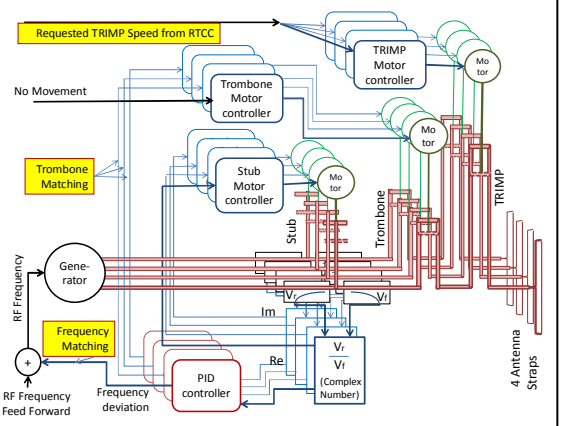

Figure 10. RF frequency variation scheme using fast trombones to maintain match.

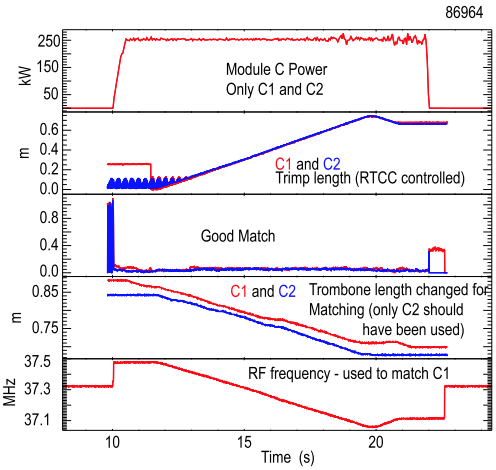

Figure 11. Fast trombones used to maintain matching during an RF frequency sweep

outputs are show. This figure illustrates how good match is maintained for both outputs throughout the pulse.

This modification has been implemented on the two JET ICRH modules (C and D) which are not equipped with 3dB couplers. Real time ICRH frequency variation has therefore become available for these two modules in addition to the module (B) which was used in the experiments reported in [44]. The decision has been taken to leave the frequency variation scheme used in [44] unchanged for module B, as this scheme allows more rapid tuning of the ICRH frequency over a small frequency range. With this modification significantly more ICRH power is available for real time sawtooth control on JET. The main limitations for the use of this control scheme do, however, remain:

i) The very limited range of variation of the RF frequency means that the Ion Cyclotron resonance can only be moved by 5-10cm. If this method has to be implemented on ITER the range of variation needs to be significantly increased.

ii) The slow speed of the slow trombones means that changing the frequency over its full range takes about 10s. This slow response is likely to pose much less of a problem on ITER where the required sawtooth period is likely to be measured in tens of seconds.

3.3.3. Low Field Side ICRH Resonance

As mentioned, earlier JET sawtooth control experiments have focused on phased ICRH injection with the ion cyclotron resonance located precisely near the high field side (HFS) q=1 surface. On ITER only low field side (LFS) ICRH will be available for sawtooth control and the efficiency of this scheme had never been tested. Recent theoretical advances [31-32] showing that ICRH affect the sawteeth mainly via a fast ion effects and less through changing the local shear at the q=1 surface indicate, however, that LFS ICRH should be able to shorten sawteeth. To test this theory recent sawtooth control experiments on JET have been using ICRH deposited near q=1 on the low field side [2]. These experiments have demonstrated, for the first time, that such low field side ICRH, can be used for sawtooth control, shortening

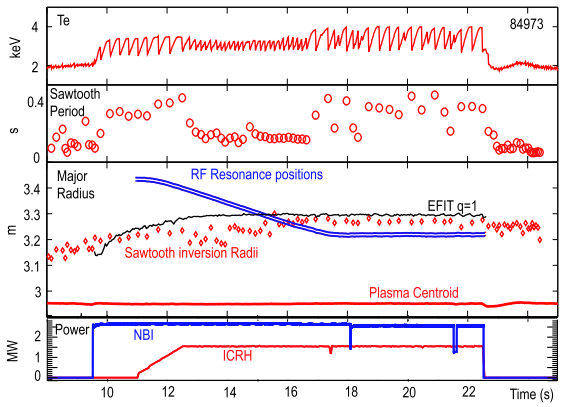

Figure 12. Sawtooth Control with LFS ICRH. The best

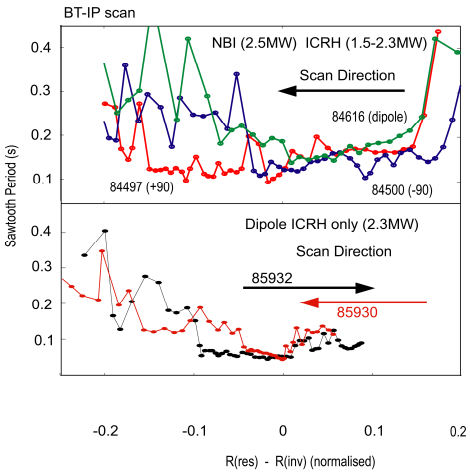

Figure 13. The Sawtooth period shown as a function of the distance of the ICRH resonance from the LFS sawtooth inversion radius.

Top box: with NBI power and three different ICRH phasing.

Bottom Box: Dipole ICRH only.

sawteeth lengthened by central fast NBI (neutral beam injection) ions. Moreover, these experiments, again for the first time, demonstrated that current drive phasing of the antennae is not needed in order to shorten the sawteeth in contrast with what has been concluded in the past when high field side ICRH has been considered. Figure 12 shows a case where sawteeth, lengthened by 2.5 MW of NBI power, are shortened by the application of 1.5 MW ICRH power with dipole phasing corresponding to a symmetric, non-current drive spectrum. In this discharge, the toroidal field and plasma current were swept, resulting in the ICRH resonance location moving slowly from off axis towards the plasma axis, passing from outside to inside the q=1 surface illustrated in the 3rd box of figure 12. Here the most reliable indicator of the location of the q=1 surface is the measured sawtooth inversion radius, indicated by red diamonds. The experiment was repeated with +90° and -90° phasing. The top box in figure 13 shows the sawtooth period as a function of the ICRH resonance position relative to the q=1 radius (represented by the sawtooth inversion radius) for the three different antenna phasings, corresponding to symmetric, co-current and counter current directed waves respectively. The bottom box shows the response of two similar discharges without neutral beam heating. In one of these discharges the plasma current and toroidal field sweep moved the resonance plasma from off axis towards the plasma centre, while the direction of the sweep was changed in the second discharge to move the resonance from the plasma centre towards the edge. In both discharges it was seen that a region where very short sawteeth could be achieved existed when the ICRH resonance was near the location of the sawtooth inversion radius. The small differences between the two ICRH only discharges are more likely to be due to small differences in plasma parameters than to have anything to do with the direction of the scan. All 5 discharges in figure 13 confirm that effective sawtooth period shortening can be achieved with the ICRH resonance located near the q=1 surface on the low field side. Subsequent to these experiments stability calculations have been performed confirming that LFS ICRH should indeed destabilise sawteeth irrespective of the phasing.

Further experiments have been carried out with much higher levels of NBI power. In these discharges it proved much more difficult to shorten the sawteeth significantly, though some modest sawtooth shortening was observed. It is likely that the lack of efficient sawtooth

shortening in this case was due to the high density naturally achieved in high power H-modes. Efficient sawtooth shortening in such plasmas is likely to require significantly higher ICRH power levels.

4. Real Time ELM and Sawtooth period measurements

Real time determination of ELM and sawtooth frequencies is a requirement for closed loop control and, even for pacing, such real time information is important to check that the pacing is effective. Though the diagnostic measurements used for this determination are different in the two cases, the algorithms determining the frequency are similar. For the ELM frequency determination used by the JET ELM frequency controller, the algorithm has been developed and tested for the first time in 2013. For this control the choice of the appropriate diagnostic signal was key, in order to detect ELMs but no other perturbations – in particular perturbations associated with pellets and kicks which do not trigger ELMs. Having looked at a variety of JET signals the choice was made to use the bolometer measurement of the total radiated power. This signal reacts much slower than the signals traditionally used to look at ELMs. For the real time control of the ELM frequency a small delay of a few milliseconds is, however, of no consequence given the desired ELM frequency range 10-100Hz and the slow response of the gas injection which it is intended to use as the actuator in closed loop experiments. The slow, rather filtered, response of the bolometer signal actually gives a significant advantage in the real time ELM frequency determination, as the sampling rate of 2 or 4 ms used in the controller would result in ELMs easily being missed in faster ELM signals. Figure 14 shows the response of a variety of signals to pellets and ELMs. The algorithm used to detect an ELM in real time looks for a rapid increase followed by a rapid decrease in the total radiated power. More details on this ELM detection can be found in [1]. Figure 15 shows the signals used for the sawtooth period determination. The traces in the top box show ECE electron temperatures at full resolution as available post pulse. The trace in the second box is the one used for the real time sawtooth detection. As can be seen this signal is not of as high quality as the post pulse ECE signals. This reduced quality is not only due to the much lower sampling rate and work is proceeding to try to have better real time electron temperature measurements. The signal is however of sufficient quality for detection of sawtooth crashes based on the step change observed in the temperature as seen in box 3 of

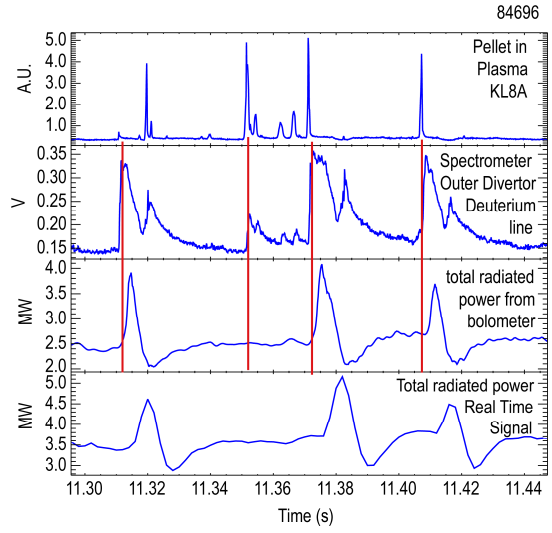

Figure 14. Pellet and ELM signals.

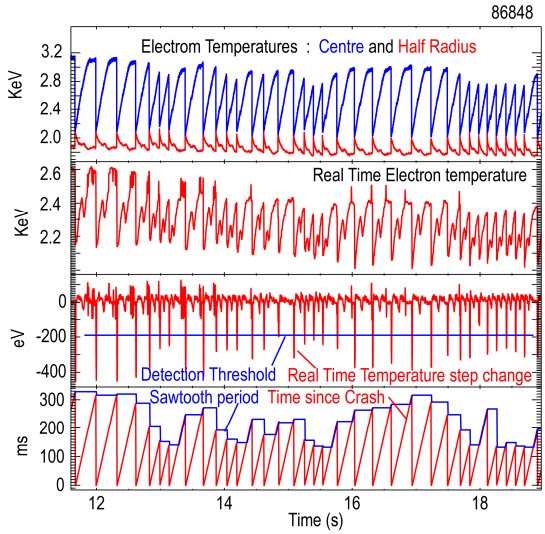

Figure 15. Sawtooth Signals.

figure 15. Having developed an algorithm to detect ELMs and sawteeth in real time the derivation of a continuous ELM period signal follows along the same lines as the real time sawtooth period determination described in [44]. In this algorithm the instantaneous ELM/sawtooth period is determined as the maximum between the time elapsed since the latest ELM/sawtooth crash and the interval between the two most recent ELMs/Sawtooth crashes. This is illustrated in the last box in figure 15. The advantage of this way of determining the period is that, in the case of an increase in period, one does not wait for the subsequent ELM/sawtooth crash for the controller to have the information that the period has increased.

5. Algorithms for Continuous Control

Though showing many similarities, the continuous control algorithms for sawtooth and ELM control, as performed at JET, are rather different due to the significant difference in the actuators and in the dynamics and linearity of the plasma response to these actuators. The basic control diagram in figure 2 which is similar for both control schemes have been expanded into more detailed diagrams in figure 16 and figure 17 showing the most recent control schemes and highlighting the differences. Due to the tradition of speaking of ELM frequency rather than ELM period, the choice was made to control a 'linearised' ELM frequency rather than the ELM period. The linearisation function in figure 16 was derived by translating the trend curves in figure 6 to show ELM frequency rather than ELM period and then inverting the resulting curves. As the two curves are identical apart from one being shifted horizontally with respect to the other, the linearisation does not depend on which of the trend curves is used to derive it. The linearisation assures that the loop gain remains constant even for

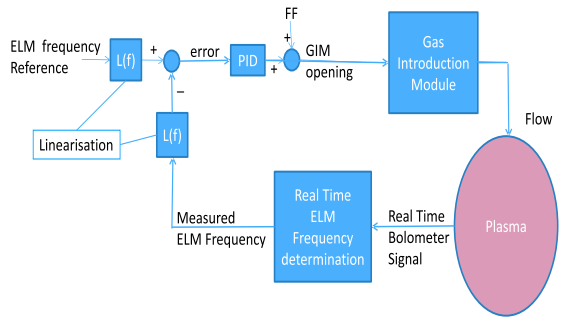

Figure 16. ELM feedback block diagram.

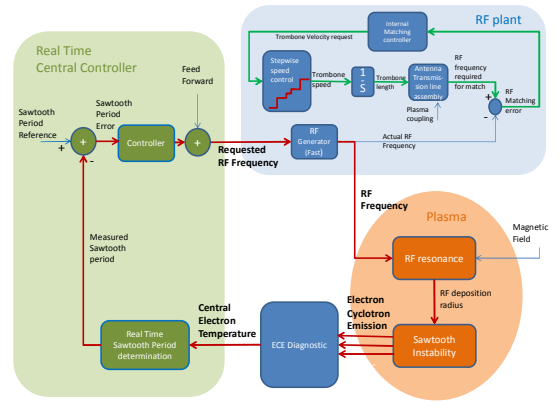

a)

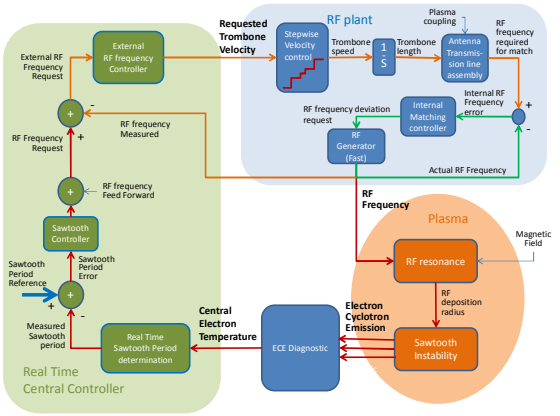

b)

Figure 17.

a) Sawtooth period feedback controller as used in the experiments in [44], showing the ICRH automatic matching loop which is used to maintain match while the frequency changes.

b) Alternative sawtooth period feedback controller, using the trombone velocity as the control actuator and relying on the internal matching to change the RF frequency.

significant changes in the required and measured ELM frequencies. For the sawtooth controller the choice has remained for the control of sawtooth period and the main changes in the most recent controller have been implemented to take account of the changes to the way the ICRH frequency can now be indirectly controlled by asking the trombones to move and letting the internal ICRH matching system modify the generator frequency in response, as described in section 3.3.2 above.

Figure 17a shows how the ICRH automatic matching was imbedded within the overall control scheme used in for the experiments described in [44]. In this diagram, the automatic matching system has been shown in a simplified version. Firstly, the stub control is not shown, since the stub movement required to compensate for a frequency change is negligible compared to the required trombone movement. This means that the stub controller will hardly require any change in stub position when the frequency changes within the modest range available. The frequency range is therefore determined by the available trombone variation alone. A second simplification which has been introduced in figure 17a, is that the error signal of the internal matching loop is considered to be derived as the difference between the 'RF frequency required for match' and the actual frequency. This approach is justified as, for any trombone position, an RF frequency exists which would result in a match. In fact, over the limited frequency range considered, the 'RF frequency required for match' can be considered to be a linear function of the trombone length and therefore it is justified to consider the trombone position in terms of this notional 'RF frequency required for match'.

In this control scheme, as already mentioned, the stepwise control of the trombone motors means that, if the fastest possible frequency variation and therefore the fastest trombone movement is required, the frequency error signal has to be rather large. This in turn results in significant power being reflected towards the generator. As described in section 3.3.1, only one of the JET RF generators (module B) can work with such high reflection. Figure 17a shows how the sawtooth control loop (red lines) is separate from the matching loop (green lines) in this mode of operation.

Taking advantage of the indirect RF frequency control described in 3.3.2, a new sawtooth controller, shown in figure 17b has been designed. To retain the architecture of the main sawtooth period controller, an internal RF frequency control loop has been embedded in the overall control loop. This internal loop takes the RF frequency reference signal from the output of the Sawtooth controller and controls the actual RF frequency in a closed loop by using the RF trombone velocity as the actuator. Figure 17b shows how the three control loops are nested inside each other in this scheme, with the sawtooth period loop indicated by red lines, the RF frequency loop indicated by orange lines and the matching loop indicated by green lines.

6. Closed loop control – Simulations and Experiments

In order to tune the controllers prior to testing them in earnest in JET pulses, simple simulators aimed at capturing only the main dynamics have been built into the control algorithms. In these simulators, the plasma dynamics is considered to be so fast that it can be ignored and the plasma can therefore be represented by its steady state, non-linear response. All the dynamics are assumed to be associated with the actuators. The plasma behaviour is simulated by assuming that a certain actuator state can be directly translated, using a non-linear input output map, into an instantaneous ELM or sawtooth period. When the time since the previous ELM/sawtooth crash exceeds this period, the simulator generates a simulated

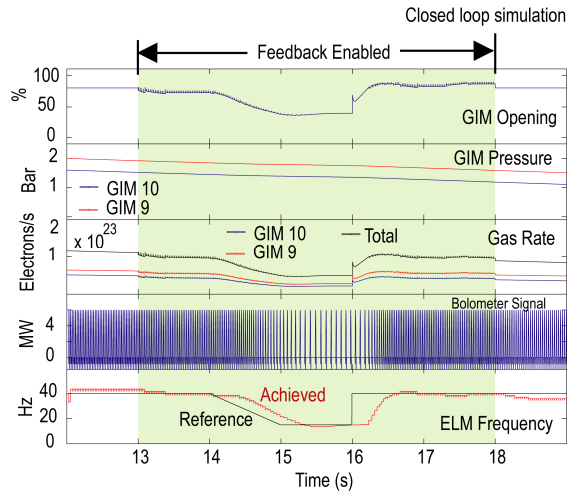

Figure 18. Simulated ELM frequency closed loop control.

ELM or a sawtooth crash. The ELM is represented by a 'spike' on the simulated bolometer signal while the sawtooth crash is represented as an abrupt decrease in the simulated central electron temperature. The temperature evolution between sawtooth crashes is modelled as a simple 1st order return towards a steady state value. The non-linear maps used for the simulations are based on open loop experiments. For the ELMs the curve in figure 6 has been used. Since the behaviour of the sawteeth is less systematic than the ELM behaviour, various input output maps have been used in the sawtooth simulation as described below. The dynamics in the simulators resides in the simulation of the actuators. For the ELM controller the dominant effect is the time taken for gas to flow from the gas injection module, through narrow pipes, to the plasma. Figure 18 shows the simulated closed loop behaviour of the ELM controller, assuming the use of two gas introduction modules (GIM 9 and GIM10) both controlled by the same controller output but operating at different pressures. The simulator models the pressure drop throughout the gas injection and based on this pressure and the requested gas valve opening it simulates the ELM frequency evolution. Further details of the ELM control simulations can be found in [1].

The ELM controller has been operated recently, demonstrating closed loop control of the ELM frequency, via real time variation of the injected gas flow for the first time [1]. This controller has been used in conjunction with ELM pacing techniques allowing the injected gas to be successfully replaced by pellets, while maintaining the ELM frequency. Operating in this way guaranteed that the ELM frequency did not drop too low, even if the pellets were not sufficiently reliable. The pellet triggering of ELMs is seen as a perturbation which increases the ELM frequency. The ELM controller responds by reducing the gas flow. Figure 19 shows an example where the ELM frequency is kept close to the requested value despite a number of disturbances. Initially, an abrupt impurity influx decreases the ELM frequency and the

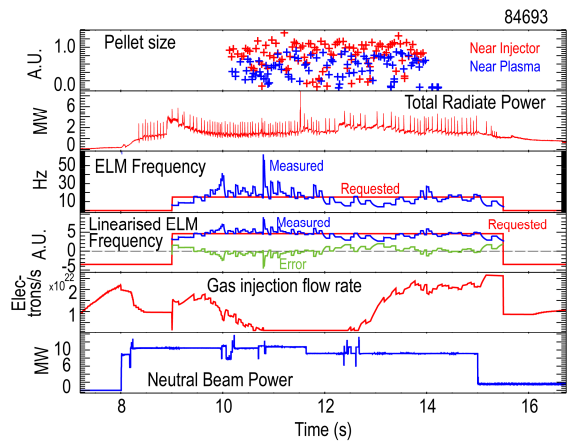

Figure 19. ELM frequency feedback controller response to pellet injection.

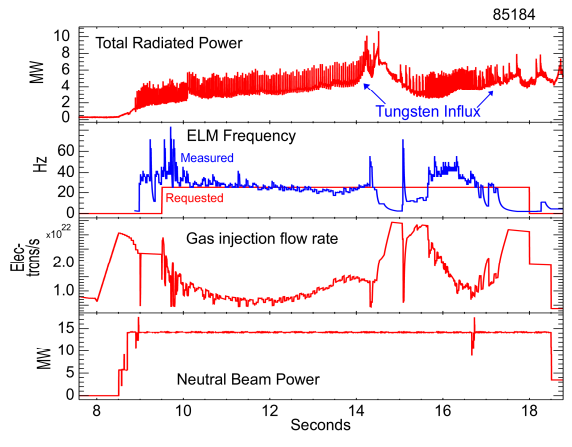

Figure 20. ELM frequency feedback controller response to strong tungsten influx.

controller responds by injecting more gas, then the injection is slowly decreased as the effect of the impurities disappears. The injection is further reduced almost to zero as pellets are injected. Between 11 and 12 seconds the plasma configuration is changed by moving divertor 'strike point' resulting in a reduced natural ELM frequency and an associated reduction in the ability of the pellets to trigger ELMs. The controller responds again bringing the ELM frequency back to the desired value. In figure 19 the top box shows a measurement of the pellet size at two points along the flight line. This measurement indicates the strong scatter in pellet size and the reduction in average pellet size as the pellets fly through the injection line. The second box shows measured and requested ELM frequencies, while the third box shows the linearised ELM frequencies (requested and measured) together with the error signal used as input to the PID controller. The error signal stays nicely near zero showing efficient control. Figure 20 gives a more extreme example of the operation of the ELM frequency controller. In this discharge a significant influx of Tungsten occurs around 14 seconds resulting in a dramatic reduction of the ELM frequency. The controller responds by injecting the maximum amount of gas and it succeeds in rescuing the discharge, which would almost certainly have disrupted otherwise. After an overshoot in ELM frequency, the frequency returns to the desired value, before a second tungsten influx occurs shortly before the end of the high power phase. The tungsten influx problems in this discharge are almost certainly associated with operating at too low requested ELM frequency (20Hz) and indicate that more stable operation would require that the requested ELM frequency is increased.

For the sawtooth control simulations the dynamics is governed by the trombone movement, with the maximum trombone speed being dominant. Figure 21 shows two different input output maps used for the simulations in the following. One of these maps crudely represents the continuously varying sawtooth period with a minimum when the RF resonance is near q=1, as observed in the experiments in [44], while the other map assumes an abrupt switch in sawtooth period as seen in the above experiments and in the experiments reported from Tore Supra [39-40]. Figure 22 shows a simulation of the expected closed loop behaviour under the assumption of a

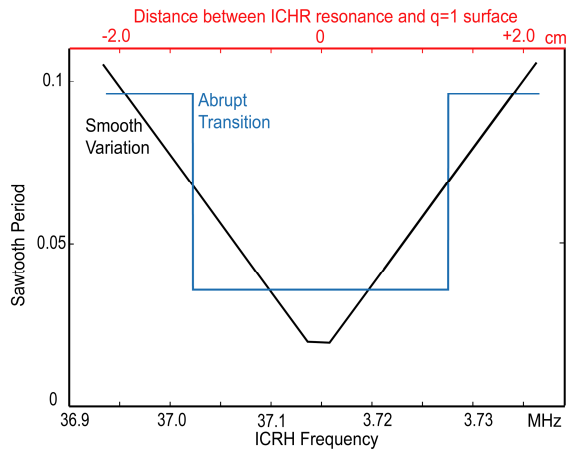

Figure 21. Steady state input output maps assuming either smooth or abrupt variation in sawtooth period.

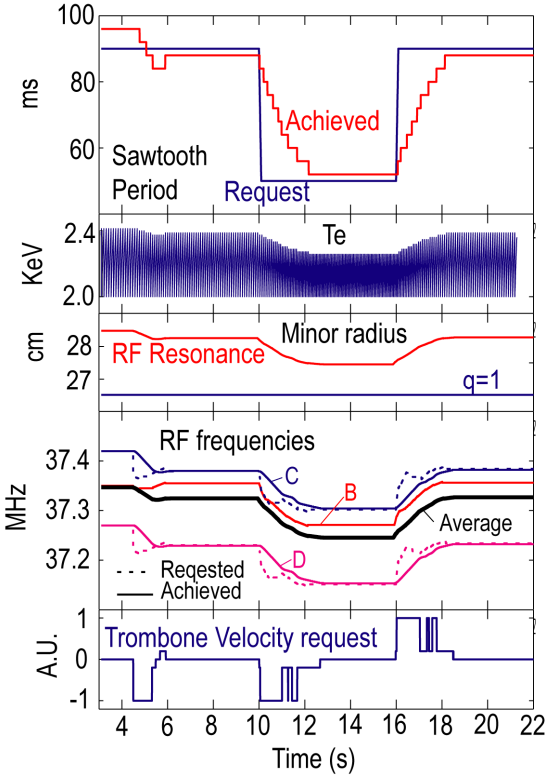

Figure 22. Simulated sawtooth period control, assuming 'smooth' input output map.

smoothly varying sawtooth period. In this simulation, it is assumed that three ICRH generators are used (B, C and D). C and D are controlled using the new method of varying the ICRH frequency (figure 17b), while it is assumed that generator B is still using the old method (figure 17a). The advantage of this way of operating is that a small variation of the frequency in generator B can happen very rapidly, allowing fast fine control. In the simulation it is assumed that the sawtooth period is governed by the power averaged location of the ion cyclotron resonances from the three generators. The dotted lines in the fourth box show the requested RF frequencies in the internal frequency loops for generators C and D, while the full lines show the achieved RF frequencies. The full black line shows the power averaged frequency. The third box shows the averaged resonance location relative to the q=1 surface while the top box shows the requested and simulated sawtooth period. This simulation shows that, given a smooth input output map, a good control of the sawtooth period should be achievable.

Figure 23 shows a repeat of the above simulation under the assumption of the more abrupt input output map. For simplicity, only module C and D have been included in this simulation and the loop gain has been reduced to avoid too violent oscillations. Not surprisingly it was not possible to completely avoid the observed oscillations by reducing the gain, with a gain reduction only resulting in the oscillation frequency being reduced. As it is the aim of the controller to maintain sufficiently short sawteeth without a single sawtooth being long enough

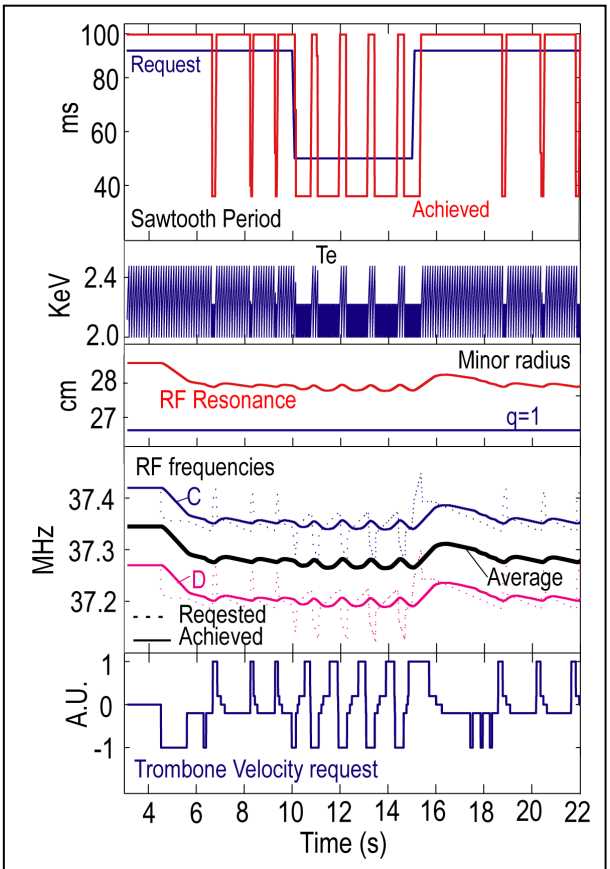

Figure 23. Simulated sawtooth period control, assuming 'abrupt' input output map.

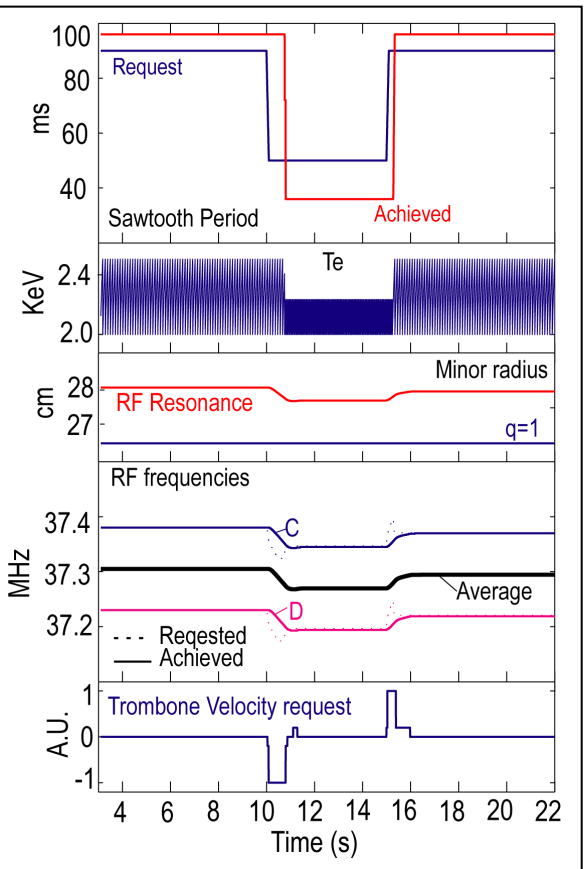

Figure 24. Simulated sawtooth period control, assuming 'abrupt' input output map and introducing a dead band around the requested period.

to trigger an NTM, such an oscillatory controller is unlikely to be effective. Figure 24 shows the result of introducing a fairly large 'dead band' around the requested sawtooth period. As long as the sawtooth period is within this dead band the control error is set to zero. Figure 24 shows that such a controller should be able to switch between short and long sawteeth, as desired. It is, however, unlikely that this scheme can efficiently assure short sawteeth, as it does not give any warning that one is moving closed to the point of switching to long sawteeth. On ITER, where the acceptable sawtooth period is likely to be tens of seconds, it is possible that the controller can have time to react early within the first long sawtooth when the transition to long sawteeth happens. In this case it is possible that intermediate length sawteeth can be achieved even with an abrupt input output map. Another way to cope with an abrupt input output map is to proceed as in [39], implementing real time sawtooth inversion radius determination and controlling the RF resonance position relative to the measured inversion radius. The abrupt transitions between long and short sawteeth seen in figure 12, which are reminiscent of the observations on Tore Supra [39], does have the advantage that the available frequency range, though small, is likely to be sufficient to allow the desired sawtooth period control as long as the problems of oscillations described above are solved.

Limited experimental time has prevented the newly developed way of controlling the RF frequency to be employed for real time control of the JET sawtooth period. Hopefully experimental time will become available over the next years to test the sawtooth period controllers developed and described above on JET.

7. Conclusions

The installation of the ITER like, all metal, wall on JET has highlighted the need to limit the influx and accumulation of heavy metallic impurities in the plasma. Control of the ELM and sawtooth instabilities plays a key role in achieving this goal. In addition, controlling ELMs and sawteeth, remains important to limit divertor heat load and to avoid triggering of neoclassical tearing modes.

In this paper the work, mainly on JET, exploring ways of controlling ELMs and sawteeth has been described, highlighting that a number of parallels exists between the engineering of controllers for these two instabilities.

Repetitive triggering of ELMs with radial field 'kicks' and pellets have been extensively explored on JET as described. Such methods have also been demonstrated to be reliable for sawtooth control on TCV using ECRH modulation while it would be of interest to attempt to use modulated ICRH for sawtooth control on JET.

Extensive work to develop continuous ELM and sawtooth controllers has proceeded along parallel lines on JET with efficient ELM frequency control, using gas injection as the actuator, having been demonstrated in 2013-14. This controller has become an important asset for JET operation and, though gas injection is unlikely to be effective in affecting ELMs on ITER, similar controllers could be developed using other actuators such as pellets and resonant magnetic perturbation coils. It would be of interest to test such controllers on existing machines and the present controllers could probably readily be transformed into using these actuators.

For sawtooth control the work has mainly focused on improving the ability of changing the ICRH frequency in real time and JET is now able to change the ICRH frequency, all be it slowly and over a small range, in real time on all the RF antennae, without losing the required matching. Simulations indicate that, with these improvements, it should be possible to extend

the operation of the real time sawtooth period controller published in 2011, to plasmas where the sawtooth period is increased by the presence of high energy ions from neutral beam injection. Hopefully demonstration of such closed loop control can be done over coming years. The ability to vary the ICRH frequency in real time, though designed with the aim to control the sawtooth period, could prove to have a number of other applications.

In addition to the real time work, the demonstration that ICRH power deposited near the q=1 surface on the low field side of the plasma can shorten sawteeth, is encouraging for ITER, where only LFS deposition will be possible. Achieving effective sawtooth shortening in high density, high power H-mode plasmas have proven more of a challenge and it is likely that more ICRH power will be required. Whether a similar increase in the actuator power would be required in the case of using ECRH for sawtooth control is not clear and it would therefore be important to test the use of ECRH for sawtooth control in high power H-modes. Though the sawtooth shortening achieved in high power JET H-modes is modest, it is encouraging that the ICRH absorption location required to achieve this shortening also is favourable for the avoidance of the accumulation of heavy impurities in the plasma centre.

More routine use of the developed schemes using gas and pellets for ELM control and ICRH for sawtooth control, are likely to be key to allow more stable high performance JET discharges with minimal tungsten content. Achieving such stable dischargers reliably is essential as JET moves towards a period of operation with Deuterium-Tritium plasmas, with the aim of demonstrating steady production of significant fusion power over at least 5 seconds.

In ITER and ideally also on JET, these control schemes have to be run together with a number of other controllers in an integrated control system. Integration of a variety of controllers to control a range of mutually coupled plasma instabilities and properties will be required for the operation of future tokamaks. Gaining such experience on JET and other current tokamaks is essential to be able to go into ITER operation with confidence.

Acknowledgements

This work has been carried out within the framework of the EUROfusion Consortium and has received funding from the Euratom research and training programme 2014-2018 under grant agreement No 633053. The views and opinions expressed herein do not necessarily reflect those of the European Commission.

References

[1] M. Lennholm et al, 'ELM frequency feedback control on JET', submitted to Nucl. Fusion. (2014)

[2] J. Graves, M. Lennholm 'Sawtooth control in JET with ITER relevant low field side resonance ICRH and ITER like wall', accepted for publication in Plasma Physics and Controlled Fusion. (2014)

[3] M. Keilhacker, Plasma Phys. Control. Fusion, vol. 26, 49 (1984).

[4] V. Erckmann et al, Phys. Rev. Letters, vol. 70, 2086 (1993).

[5] H. Zohm, Plasma Phys. Control. Fusion, vol 38, 105 (1996).

[6] A. Loarte et al., Plasma Phys. Control. Fusion, vol. 45, 1549 (2003).

[7] K. Kamiya et al., Plasma Phys. Control. Fusion, vol. 49, S43 (2007).

[8] S. von Goeler, W. Stodiek and N. Sauthoff, Phys. Rev. Letters, vol. 33, p. 1201, (1974).

[9] M. N. Bussac, R. Pellat, D. Edery and J.L Soulé, Phys. Rev. Letters, vol. 35, p. 1638, (1975).

[10] M. D. Kruskal and C. R. Oberman, Phys. Fluids, vol. 1, p. 275, 158.

[11] F. Porcelli, D. Boucher and N. N. Rosenbluth, Plasma Phys. Control. Fusion, vol. 38, p. 2163, (1996).

[12] R. B. White, P. H. Rutherford, P. Colestock and M. N. Bussac, Phys. Rev. Letters, vol. 60, p. 2038, (1988).

[13] R. B. White, M. N. Bussac, F. Romanelli, Phys. Rev. Letters, vol. 62, p539 (1989)

[14] R. B. White, F. Romanelli, M. N. Bussac, Phys. Fluids B, vol. 2, p745 (1990).

[15] B. Coppi, P. Detragiache, S. Migliuol, F. Pegoraro and F. Porcelli, Phys. Rev. Phys. Rev. Letters, vol. 63, p. 2733, (1989).

[16] F. Porcelli, Plasma Phys. Control. Fusion, vol. 33, p.1601, (1991).

[17] A. Loarte et al., Nucl. Fusion, vol. 54, 03300, (2014)

[18] G. Federici et al., Plasma Phys. Control. Fusion, vol. 45**,** 1523, (2003)

[19] G. Saibene et al. JNM V.241–243, 476, (1997).

[20] M.N.A. Beurskens et al., Nucl. Fusion, vol. 54, 04300, (2014)

[21] P.T. Lang et al., Nucl. Fusion, vol. 44**,** 665, (2004)

[22] P.T. Lang et al., Nucl. Fusion, vol. 51, 033010, (2011)

[23] L.R. Baylor et al., Phys. Rev. Letters, vol. 110, 245001, (2013)

[24] A. Geraud et al., Fusion Eng. Des., Vol. 88, 1064-1068, (2013)

[25] A.W. Degeling, Y.R. Martin, J.B. Lister, L. Villard, V.N. Dokouka, V.E. Lukash and R.R. Khayrutdinov, Plasma Phys. Control Fusion, 45, 1637, (2003)

[26] P.T. Lang et al. and ASDEX Upgrade Team, Plasma Phys. Control. Fusion, vol. 46, L31. (2003)

[27] F. Sartori, P. Lomas, F. Piccolo, M.K. Zedda and JET EFDA contributors, 35th EPS Conf. on Plasma Physics (Hersonissos, Crete, Greece) 2008, http://eps2008.iesl.forth.gr/index.html. (2008)

[28] F. Romanelli et al., and JET-EFDA, Culham Science Centre, Abingdon, Oxfordshire OX14 3DB, UK JET-EFDA Contributors, Fusion Eng. Des., Vol. 84, 150, (2009)

[29] E. de la Luna, APS–DPP Meeting (Atlanta, USA, 2009), PI2.00002, (2009) see http://meetings.aps.org/Meeting/DPP09/Event/109696

[30] L.-G. Eriksson et al., Phys. Rev. Lett., vol. 92, p. 235004, (2004).

[31] J. P. Graves, I. T. Chapman, S. Coda, M. Lennholm, M. Albergante and M. Jucker, Nature Comms., vol. 3, p. 626, (2012).

[32] J. P. Graves, I. Chapman, S. Coda, L.-G. Eriksson, and T. Johnson, Phys. Rev. Lett, vol. 102, p. 065005, (2009).

[33] J.P. Graves et al., Nucl. Fusion, vol. 50, p. 052002, (2010).

[34] L.-G. Eriksson et al., Nucl. Fusion, vol. 46, p. S951, (2006).

[35] C. Angioni, T.P. Goodman, M.A. Henderson and O. Sauter, Nucl. Fusion, vol. 43,p. 455, (2003).

[36] A. Mück et al, Plasma Phys. Control. Fusion, vol. 43, p. 1633, (2005).

[37] I. T. Chapman, Plasma Phys. Control. Fusion, vol. 53, p. 013001, (2011).

[38] I.T. Chapman et al. Nuclear. Fusion, vol. 52, p 063006, (2012).

[39] M. Lennholm et al., Phys. Rev. Lett. 102, 115004, (2009).

[40] M. Lennholm et al., Fusion Sci. and Tech., vol. 55, p 45. (2009).

[41] J. I. Paley et al., Plasma Phys. Control. Fusion, vol. 51, p. 055010, (2009).

[42] J. I. Paley et al., Plasma Phys. Control. Fusion, vol. 51, p. 055010, (2009).

[43] G. Witvoet et al., Nucl. Fusion, vol. 51, p. 073024, (2011).

[44] M. Lennholm et al., Nucl Fusion, 51, 073032 (2011).

[45] F. Romanelli and JET EFDA Contributors, Nucl. Fusion, vol. 53, 104002, (2013)

[46] G.F. Matthews et al., Physica Scripta, 014001. (2011)

[47] R. Neu et al., Physics of Plasmas, vol. 20. 056111, (2013)

[48] G. Matthews et al, proc. PSI, (2013).

[49] E. Joffrin et al., Nuclear Fusion, vol. 54, 013011, (2014)

[50] M.N.A. Beurskens, J. Schweinzer et al., Plasma Phys. Control. Fusion, vol. 55, 124043. (2013)

[51] T. Pütterich, R. Dux, R. Neu et al., Plasma Phys. Control. Fusion, vol. 55, 124036, (2013)

[52] R. Dux et al., JNM 390-391, 858. (2009)

[53] I. Chapman et al, Nucl. Fusion, vol. 50, 102001, (2010).

[54] T. P Goodman et al., Phys. Rev. Letters, vol. 106, p. 245002, (2011).

[55] G. Witvoet et al., Nuclear Fusion., vol. 51, p.103043, (2011).

[56] M. Lauret et al., Nuclear Fusion, vol.52. 062002, (2012),

[57] A. Loarte et al. Phys. Plasmas, vol. 11, 2668, (2004)

[58] E. Solano et al., Proc. 41st EPS Conference on Plasma Physics, Berlin, Germany, June 2014, P. 1.006, (2014) see http://ocs.ciemat.es/EPS2014PAP/pdf/P1.006.pdf

[59] D. Frigione et al. 21st International Conference on Plasma Surface Interactions(PSI 21), Kanazawa, Japan, 2014 (2014).

[60] T. Evans et al., Nature Phys., vol. 2, p 419. (2006)

[61] M. Mori et al., Plasma Phys. Cont. Fuison, Vol. 38, 1189, (1996)

[62] S. J. Fielding et al., Proc. 28th EPS Conf. on Plasma Physics (Funchal, Portugal), vol 25A (ECA), 1825. (2001)

[63] T. Evans et al., Phys. Rev. Lett., vol. 92 ,235003, (2004)

[64] Y. Liang et al., Plasma Phys. Control. Fusion, vol. 49, B581, (2007)

[65] V. Riccardo et al., Nucl. Fusion, vol. 49, 055012, (2009).

[66] D. McDonald et al., Fusion Science and Technology, vol. 53, p89, (2008)

[66] F. Bouquey et al. 'Test Bed Validation of the Tore Supra Electron Cyclotron Launcher Upgrade' SOFT 2014, San Sebastian, Submitted for publication in Fusion engineering and design.

[67] J. Bucalossi et al., Fusion Eng. Des. Vol. 89, p907, (2014)

[68] Q. King and H. Brelen, 'An Experimental Automatic Control Facility at JET', JET preprints JET-P(98), (1998).